

Discovery of neuroprotective agents that inhibit human prolyl hydroxylase PHD2

Nicole L. Richardson, Laura J. O'Malley, Daniel Weissberger, Anthony Tumber, Christopher J. Schofield, Renate Griffith, Nicole M. Jones, Luke Hunter

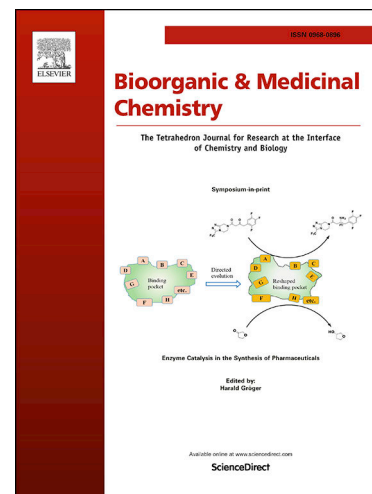
PII: S0968-0896(21)00123-1
DOI: <https://doi.org/10.1016/j.bmc.2021.116115>
Reference: BMC 116115

To appear in: *Bioorganic & Medicinal Chemistry*

Received Date: 29 January 2021
Accepted Date: 13 March 2021

Please cite this article as: N.L. Richardson, L.J. O'Malley, D. Weissberger, A. Tumber, C.J. Schofield, R. Griffith, N.M. Jones, L. Hunter, Discovery of neuroprotective agents that inhibit human prolyl hydroxylase PHD2, *Bioorganic & Medicinal Chemistry* (2021), doi: <https://doi.org/10.1016/j.bmc.2021.116115>

This is a PDF file of an article that has undergone enhancements after acceptance, such as the addition of a cover page and metadata, and formatting for readability, but it is not yet the definitive version of record. This version will undergo additional copyediting, typesetting and review before it is published in its final form, but we are providing this version to give early visibility of the article. Please note that, during the production process, errors may be discovered which could affect the content, and all legal disclaimers that apply to the journal pertain.



Discovery of neuroprotective agents that inhibit human prolyl hydroxylase PHD2

Nicole L. Richardson,^a Laura J. O'Malley,^b Daniel Weissberger,^a Anthony Tumber,^c Christopher J. Schofield,^c Renate Griffith,^a Nicole M. Jones^{b,*} and Luke Hunter^{a,*}

^a School of Chemistry, University of New South Wales (UNSW), Sydney, Australia.

^b School of Medical Sciences, University of New South Wales (UNSW), Sydney, Australia.

^c Chemistry Research Laboratory, 12, Mansfield Road, Department of Chemistry, University of Oxford, OX1 3TA, United Kingdom.

* n.jones@unsw.edu.au; l.hunter@unsw.edu.au

ABSTRACT

Prolyl hydroxylase (PHD) enzymes play a critical role in the cellular responses to hypoxia through their regulation of the hypoxia inducible factor α (HIF- α) transcription factors. PHD inhibitors show promise for the treatment of diseases including anaemia, cardiovascular disease and stroke. In this work, a pharmacophore-based virtual high throughput screen was used to identify novel potential inhibitors of human PHD2. Two moderately potent new inhibitors were discovered, with IC₅₀ values of 4 μ M and 23 μ M respectively. Cell-based studies demonstrate that these compounds exhibit protective activity in neuroblastoma cells, suggesting that they have the potential to be developed into clinically useful neuroprotective agents.

INTRODUCTION

Exposure to mild hypoxia can give a variety of benefits in health and medicine. Some athletes subject themselves to intermittent hypoxia to enhance their endurance and performance.¹ In the medical field, exposure to mild hypoxia is reported to have positive effects in diseases ranging from chronic heart and lung diseases to iron-deficiency and anaemia.^{2,3} Neuroprotective effects have also been demonstrated: intermittent hypoxia can improve walking function in patients suffering from an incomplete spinal cord injury;⁴ it can alleviate short term memory deficits in patients with mild cognitive impairments;⁵ and hypoxic postconditioning can improve function in animal models of stroke.⁶

Many of these protective effects may involve the chronic hypoxic response,^{7,8} a biochemical system in which the transcription factors known as hypoxia inducible factors (HIFs) play a key role. HIF is

a α,β -heterodimer, comprising an oxygen-sensitive alpha subunit (HIF- α) that under normoxic conditions localizes in the cytoplasm and a constitutively-expressed beta subunit (HIF- β) that localizes in the nucleus.^{9,10} Under hypoxic conditions, HIF- α accumulates, leading to its translocation into the nucleus, where it dimerizes with HIF- β . The heterodimeric α,β -HIF complex binds to hypoxia response elements leading to enhanced expression of various hypoxia-inducible genes involved in ameliorating the response to hypoxia.^{11–14} In humans there are three HIF- α isoforms (HIF-1 α –3 α), which have different and at least to some extent, context dependent roles in upregulating expression of gene sets. HIF target genes include vascular endothelial growth factor, which promotes angiogenesis and neurogenesis;^{15–17} erythropoietin, which stimulates red blood cell production and reduces blood-brain barrier leakage;^{18,19} pyruvate dehydrogenase kinase-1, which reduces mitochondrial oxygen consumption;²⁰ and glucose transporter-1, which returns the cell toward normal metabolism and glucose transport.²¹

Under normoxic conditions, HIF- α is rapidly degraded in the cell.²² The degradation process begins with the hydroxylation of two proline-residues located in oxygen dependent degradation domains of in HIF-1 α and 2 α . The presence of these hydroxyl groups promotes binding of HIF-1 α to the von Hippel-Lindau protein, which is part of a ubiquitin E3 ligase complex, leading to proteasomal degradation of HIF-1 α .^{23–26} The hydroxylation of HIF- α is catalyzed by prolyl hydroxylase (PHD) enzymes (Figure 1a).²³ The PHDs are dependent on a ferrous iron cofactor and the cosubstrates 2-oxoglutarate, and molecular oxygen (Figure 1b).²⁷ In the proposed PHD mechanism, molecular oxygen coordinates directly to the single Fe(II) ion in the PHD active site, and it ultimately provides the oxygen atom of the hydroxyl group that becomes attached to Pro564 of HIF- α .²⁸ The oxygen dependence of PHDs is the key feature that enables the hypoxic response to be activated under the appropriate conditions.²⁹

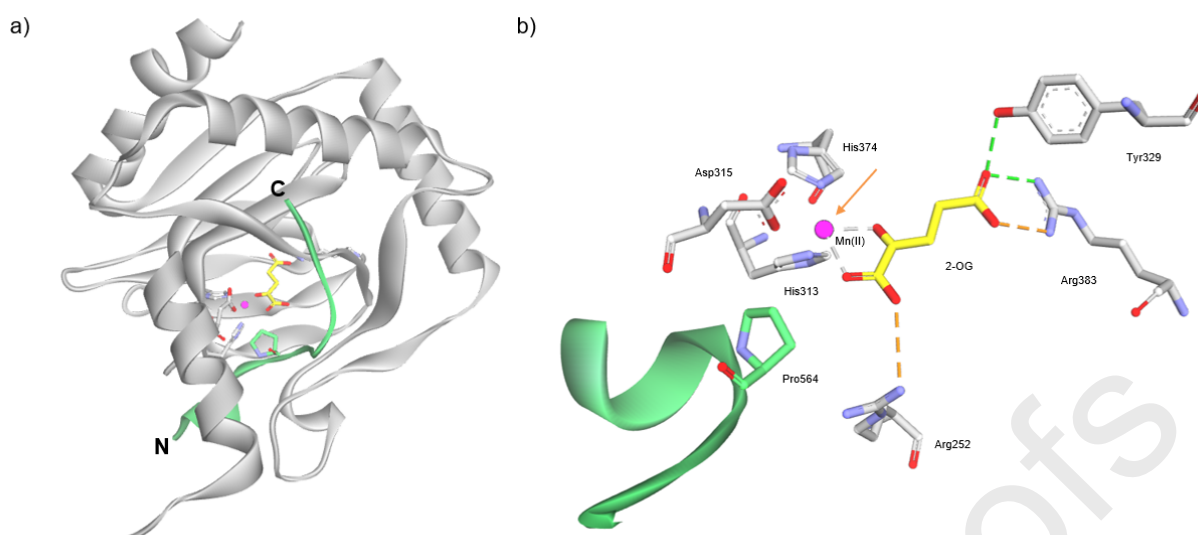


Figure 1: HIF- α binding by human PHD2. (a) View from a crystal structure of PHD2 (grey) bound to the C-terminal oxygen dependent degradation domain of HIF-1 α (green), with N-terminus and C-terminus labelled as N and C respectively (PDB: 5L9B).³⁰ Atoms colored by element (C in grey, N in blue, O in red). (b) The active site of PHD2 contains a metal ion (pink; Mn substituting for Fe(II) in the crystal structure) co-ordinated by two histidines, an aspartate, and in a bidentate manner by 2-oxoglutarate (yellow). The proposed site of O₂ coordination is indicated by an arrow. Salt bridges and hydrogen bonds are shown by orange and green dashed lines respectively.

There are normally three mammalian isoforms of the PHDs, but PHD2 is the most highly conserved. PHD2 is localized mainly in the cytoplasm and its expression is induced by hypoxia in a HIF dependent manner. Suppression of PHD2 by small interfering RNA upregulates HIF-1 α in normoxia.³¹ Complete deletion of PHD2 is fatal to mice, but conditional deletion leads to increased levels of vascular endothelial growth factor and erythropoietin.²³

There has been significant interest in identifying small-molecule inhibitors of PHD2, with a view to therapeutic applications of such inhibitors through their ability to upregulate the hypoxia response.^{3,32} Most inhibition studies of PHD2 have focused on the iron cofactor, with some early inhibitors either sequestering iron or competing with 2-oxoglutarate for binding to PHD2.³ For example, the iron chelator deferoxamine³³ has been investigated as a potential neuroprotective treatment for intracerebral haemorrhage as well as for neurodegenerative conditions such as Parkinson's and Alzheimer's diseases.^{34,35} However, simple iron chelators have poor selectivity because these cofactors are also used by many other cellular processes.³ Direct active site binders of PHD2 that compete with 2-oxoglutarate³⁶ are undergoing preclinical and clinical testing for diseases such as

anaemia, inflammatory diseases and heart disease.^{37,38} Such compounds bind to the active site both through chelation of iron and by competing with 2-oxoglutarate.^{32,36} The majority of known inhibitors were not designed with blood-brain barrier permeation as a priority and contain groups that replace the salt bridge interaction between 2-oxoglutarate and Arg383 (Figure 1b).³⁹ These groups usually contain a negative charge which is problematic for blood-brain barrier permeation, rendering such compounds inapplicable to the treatment of neurological diseases.^{40,41}

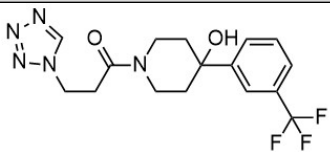
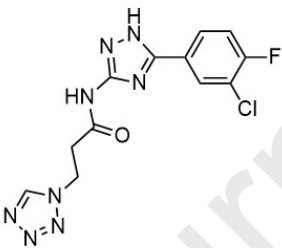
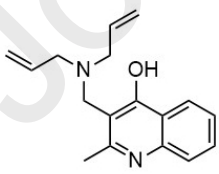
The aim of this work was to identify novel PHD2 inhibitors that could serve as lead compounds for the treatment of neurological diseases and injuries such as stroke. Herein, we describe a pharmacophore-based virtual high throughput screening approach for the discovery of such inhibitors. We also report the results of validation experiments to measure the virtual hits' PHD2 inhibitory potency and their effects on cell viability and neuroprotection.

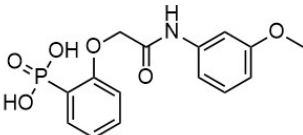
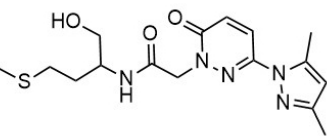
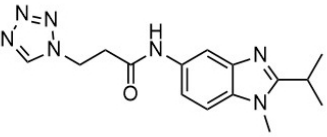
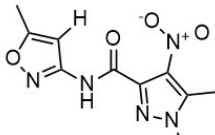
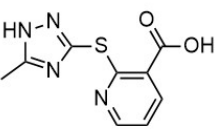
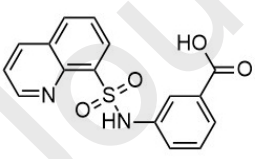
RESULTS AND DISCUSSION

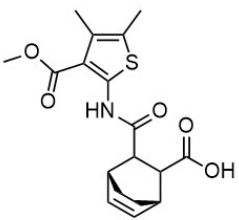
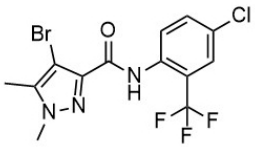
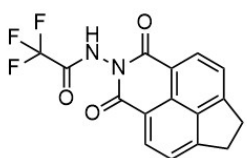
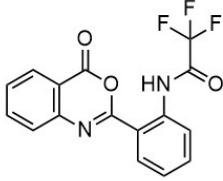
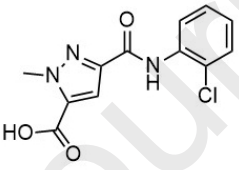
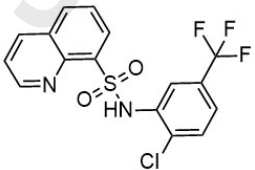
We pursued a pharmacophore-based virtual screening approach,^{42,43} because pharmacophore-based screening has been shown to be more efficient and effective than docking-based screening.^{44,45} A literature search was conducted for all crystal structures of PHD2 with an inhibitor bound, and nine pharmacophores were generated, which encode for the interactions between the inhibitor and the protein, from these crystal structures using the program LigandScout.⁴⁵ A virtual screen was then performed using compound libraries from SPECS and InterBioScreen, first including all features of the pharmacophore, then progressively lowering the number of matched features to increase the number of hits. By this means, 104 candidates that matched at least two pharmacophores were identified. We then scanned these 104 candidates using FAFDrugs4 (Free ADME-Tox Filtering Tool).⁴⁶ This tool identifies so-called pan-assay interference compounds (PAINs)⁴⁷ and assigns a toxicity risk rating to each candidate. We excluded all candidates that contained PAINs or had a risk rating higher than "low," thereby reducing the number of candidates from 104 to 72. The next step was to exclude candidates that had physicochemical properties unfavorable for blood-brain barrier permeability (e.g. molecular weight above 400 Da; number of hydrogen bond donors and acceptors greater than 3 and 7 respectively).⁴⁰ We exercised some judgement in this regard, because we assumed that there would be opportunities to subsequently improve the physicochemical properties of candidates that were slightly outside the optimal parameters. For example, we retained some candidates that contained carboxylic acid groups because we reasoned that they might subsequently be replaced with bioisosteres.³⁹ Such considerations of possible blood-brain barrier permeability narrowed the list of candidates from 72 to 42. We then docked each of these 42 candidates into a

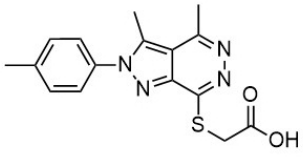
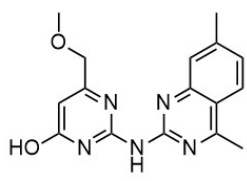
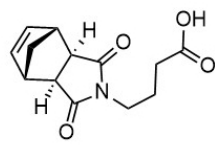
crystal structure of PHD2 (PDB: 4KBZ) using the Gold software and assessed the docked poses using ChemScore. Any compound with a docking score inferior to -30 was excluded. Amongst the remaining candidates were several families of closely related analogs, and we excluded the higher molecular weight members of such families because our priority was to discover scaffold diversity. Finally, we performed a literature search of each remaining candidate to ensure that any future medicinal chemistry development would be unencumbered by intellectual property constraints. This process delivered a final set of 18 virtual hit compounds (Table 1).

Table 1: Structures, docking scores, physicochemical properties, and PHD2 inhibitory activities of the virtual hit compounds. Physicochemical properties are color-coded based on their adherence to BBB permeability guidelines.^{a-e}

Virtual hit	Chem-Score	MW (Da) ^a	ClogP ^b	HBD ^c	HBA ^d	tPSA (Å ²) ^e	IC ₅₀ (μM)
 1	-42.4	369	0.89	1	7	84.1	>100
 2	-35.6	337	2.41	2	9	114.3	ND
 3	-40.6	268	4.10	1	3	36.4	>100

 <p>4</p>	-42.0	337	1.15	3	7	105.1	>100
 <p>5</p>	-39.8	365	-1.37	2	8	102.0	>100
 <p>6</p>	-38.9	313	2.21	1	8	90.5	>100
 <p>7</p>	-38.2	265	-1.01	1	9	118.1	>100
 <p>8</p>	-35.0	236	1.58	2	6	119.9	4.09
 <p>9</p>	-44.0	328	2.08	2	6	95.8	>100

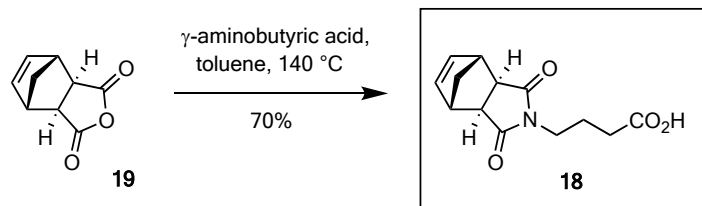
 <p>10</p>	-42.4	363	3.38	2	6	123.8	77.66
 <p>11</p>	-34.5	397	4.24	1	4	44.7	>100
 <p>12</p>	-37.9	334	2.83	1	5	66.5	>100
 <p>13</p>	-37.0	334	3.22	1	5	72.2	>100
 <p>14</p>	-35.1	280	1.89	2	6	87.1	>100
 <p>15</p>	-41.7	387	4.45	1	4	58.5	>100

 <p>16</p>	-37.6	328	3.67	1	6	77.6	26.03
 <p>17</p>	-40.7	311	2.46	2	7	96.6	>100
 <p>18</p>	-34.7	249	-0.07	1	5	74.7	>100

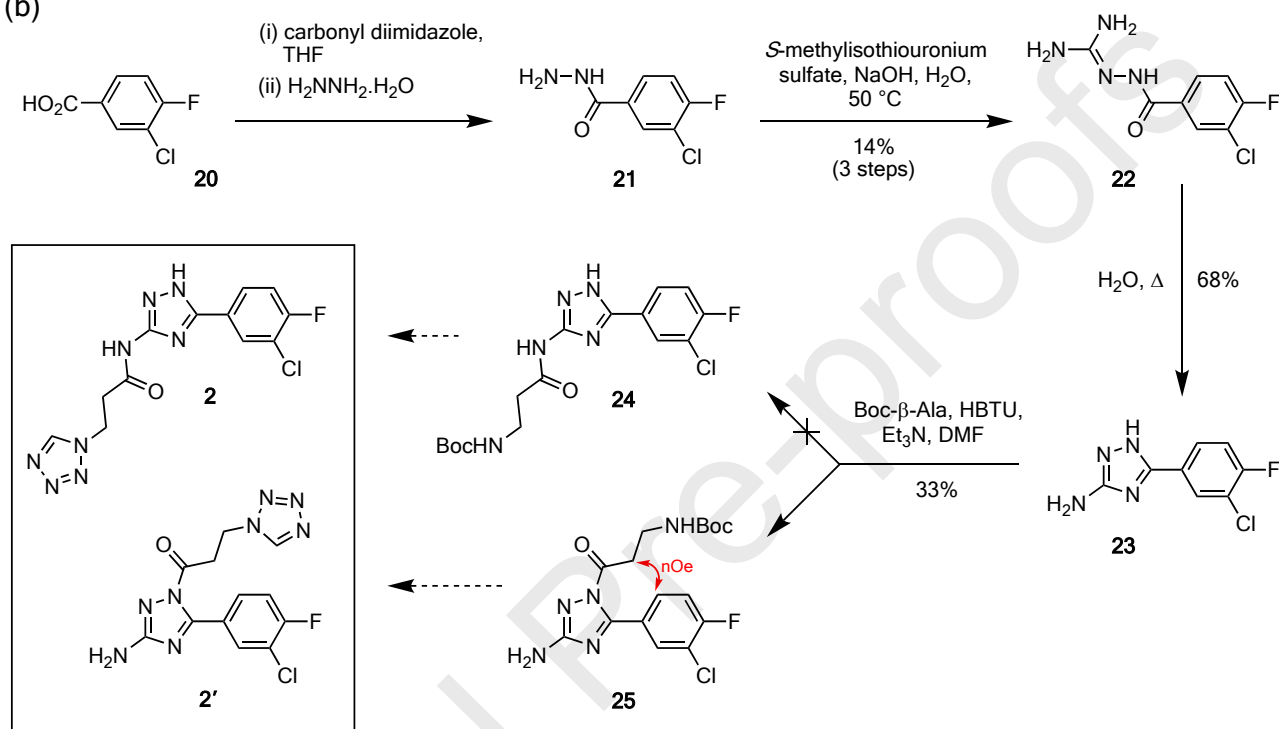
^a MW green if <400; ^b ClogP green if 1.5–2.7, yellow if 0.5–3.7, orange if outside this range; ^c HBD green if 3 or less; ^d HBA green if 7 or less, yellow if 9 or less; ^e tPSA green if <75, yellow if 75–100, orange if >100. ND: not determined

To enable the virtual hits to be validated, compounds **1–17** were purchased and compound **18** was synthesized following a literature procedure (Scheme 1a).⁴⁸ The purity and identity of each virtual hit compound was checked by NMR analysis. All compounds were found to be highly purified and of the correct structure, except for **2** which seemed to have become degraded and/or to be of the wrong constitution. No reported synthetic methods for **2** are available, so we attempted to synthesize it *via* a new route (Scheme 1b). We successfully obtained the putative precursor **23**, but further progress was thwarted when the acylation of **23** occurred not at the exocyclic primary amino group, but rather on the triazole ring (Scheme 1b); there is some precedent for the regiochemistry of such a transformation.^{49,50,51} We speculate that the commercial material that was supplied as **2** might actually have been a different structural isomer (*e.g.* **2'**, Scheme 1a). Further, it is known that ring-acylated 1,2,4-triazoles are unstable,⁵¹ and this could explain the extraneous signals that we observed in the NMR spectra of **2/2'**. We did not pursue further methods for synthesizing **2**, so this candidate was excluded from subsequent biological studies.

(a)



(b)



Scheme 1: Synthesis of potential PHD2 inhibitors. (a) Synthesis of compound **18**; (b) Attempted synthesis of compound **2**.

The virtual hit compounds **1** and **3–18** were subjected to a reported mass spectrometry-based biochemical assay to determine their ability to inhibit the hydroxylation of a peptide representing the C-terminal oxygen dependent degradation domain of HIF-1 α as catalyzed by the catalytic domain of PHD2 (aa. 181-426).⁵² Two of the virtual hits (**8** and **16**) exhibited significant inhibition of PHD2, with IC_{50} values of 4.09 μM and 26.03 μM , respectively (PHD final assay concentration: 150 nM) (Table 1). Our earlier docking results had predicted that both **8** and **16** would inhibit PHD2 by coordinating the iron cofactor and occupying the 2-oxoglutarate binding site including by interacting with Arg383, which forms a salt bridge with the C-5 carboxylate of 2-oxoglutarate within the PHD2 active site (Figure 2).

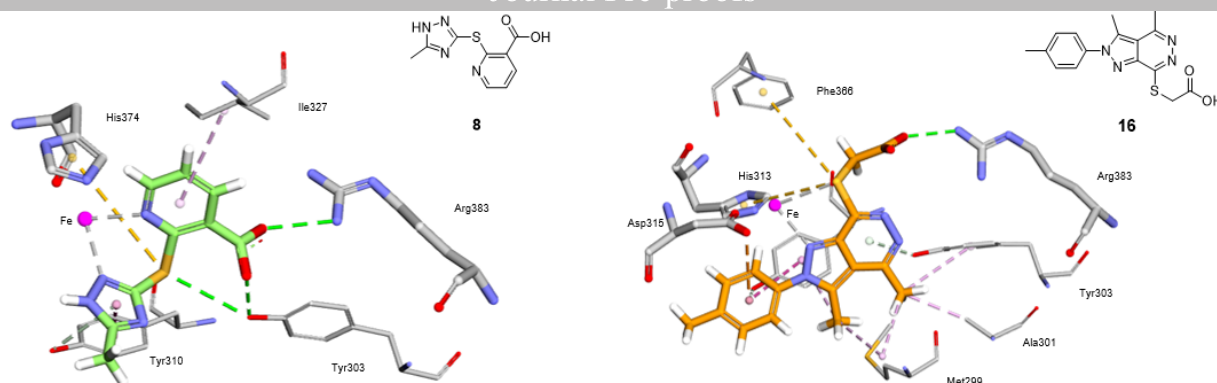


Figure 2: Docked poses of **8** (green) and **16** (orange) in the active site of PHD2. See Figure 1 for colors. Additionally, grey, yellow, green and dark and light purple dashed lines depict metal acceptor, pi-sulfur, hydrogen bond, pi-pi stacked and pi-alkyl interactions respectively.

The cellular effects of **8** and **16** were explored in SH-SY5Y neuroblastoma cells (Figure 3). The MTT cell viability assay was first used to investigate possible toxicity (Figure 3a). With this assay compound **8** was found to be essentially non-toxic at all concentrations employed, while **16** reduced cell viability only at the highest applied concentration of 100 μ M. The toxic concentration of **16** is substantially higher than the IC_{50} value of this compound (*i.e.* 26.03 μ M, Table 1). Next, the neuroprotective activities of **8** and **16** were evaluated by administering each compound in various concentrations to the cell culture then exposing the cells to oxidative stress (50 μ M H_2O_2). Manual counting of phase contrast microscopy images revealed that pre-treatment with **8** or **16** significantly reduced the rate of cell death, in a concentration-dependent fashion (Figure 3b).

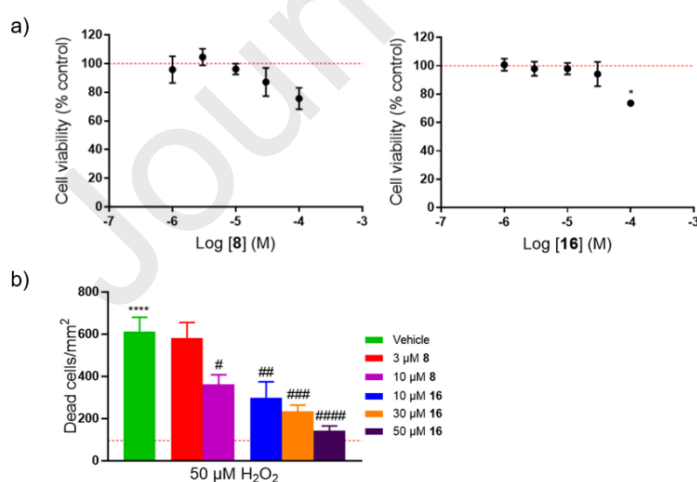


Figure 3: Effects of **8** and **16** in neuroblastoma cells. (a) MTT assays reveal that **8** and **16** are essentially non-toxic in SH-SY5Y cells at concentrations below 100 μ M; red dashed line indicates

100% viability control. (b) Compounds **8** and **16** both exhibit dose-dependent neuroprotective activity in SH-SY5Y cells when administered as a pre-treatment 2 h before H₂O₂ 50 μ m treatment; Data expressed as mean \pm SEM, from 4 separate cultures. Data analysed by one-way ANOVA (Dunnett's multiple comparisons).**** p <0.0001 vs. 100% viability control (MEM); # p <0.05, ## p <0.01, ### p <0.001, #### p <0.0001 vs. vehicle treatment; red dashed line indicates control (no pre-treatment).

CONCLUSION

We have identified two moderately potent PHD2 inhibitors through a pharmacophore-based virtual high throughput screening approach. Compounds **8** and **16** both exhibit concentration-dependent protective activity in neuroblastoma cells when administered as pre-treatments to an oxidative stress insult. The mechanism of neuroprotection by compounds **8** and **16** likely involves increasing levels of HIF-1 α , thereby upregulating the hypoxia response, although this has yet to be demonstrated. We designed our virtual screen to prioritize blood-brain barrier permeability, and while the physicochemical properties of compounds **8** and **16** are not ideal in this regard, there is scope for their future optimization through medicinal chemistry. The preliminary findings described herein could assist in the future development of treatments for neurological diseases and injuries such as stroke.

EXPERIMENTAL

Programs used: Discovery Studio Client v17.2.0.16349 (Dassault Systèmes Biovia Corp, San Diego, CA, USA); Gold Version 5.3.0 (Cambridge Crystallographic Data Centre); Maestro Version 11.3.016 (Schrödinger, LLC, New York, NY, USA); LigandScout Version 4.1.1 (Inte:Ligand, Vienna, Austria)

Generating pharmacophores: The crystal structures with PDB codes 4BQW⁵³, 4BQX⁵³, 4BQY⁵³, 4KBZ, 2HBT, 2HBU, 2G19⁵⁴ and 2G1M⁵⁴ were opened in LigandScout. Pharmacophores of each were generated by encoding the electronic and steric interactions between the bound ligand and protein as features.

Virtual high throughput screen: Digital compound libraries were acquired from SPECS (<https://www.specs.net/>) and InterBioScreen (<https://www.ibscreen.com/>). Screening was performed in LigandScout by comparing the structures of the virtual compounds with the generated pharmacophores and determining how many features are matched in each structure. Checking for

exclusion volumes was disabled, where exclusion volumes are the positions in the active site that are sterically occupied by the macromolecular environment, and all features were considered in the first screen before sequentially decreasing the number of matched features to increase the number of hits. The hits generated were analysed for multiple pharmacophore matches before subjecting to a PAINS screen (<https://fafdrugs4.rpbs.univ-paris-diderot.fr/>).

General minimisation procedure: Energy minimisations were performed in Discovery Studio after applying the CHARMM forcefield. Default settings were used except the maximum steps were changed to 10,000. Minimizations were considered converged with gradient tolerance (0.1000000 kcal/mol Å⁻¹) satisfied.

Crystal structure preparation: Crystal structures were prepared by first downloading the pdb file from the Protein Data Bank and deleting the bonds associated with the metal cation. The corrected file was then imported into DS and water molecules were removed and hydrogens added to account for any missing in the crystal structure. A three-part minimisation was performed with different components of the crystal structure constrained at each part. The first minimisation was performed on the hydrogens with all atoms fixed excluding hydrogen. The second was performed on the side chains with the backbone and ligand bound fixed. The final minimisation was performed on all amino acids outside of the active site, where the active site is a defined sphere around the ligand that encompasses the interacting amino acid residues. The ligand was then removed from the structure and the receptor was ready for docking.

Docking: Docking was performed using GOLD docking software through DS. The crystal structure ligand was docked into the crystal structure to determine efficiency of the docking method, with the method that had the closest pose and interactions to the original carried forward. The fitness function ChemScore and the default settings were used except the number of dockings was changed to 100, detect cavity was false and early termination was false. The flexibility parameters were changed from the default to increase the flexibility: explore ring conformations was changed to flip ring corners, flip ring amide bonds was set to true, flip planar R-NR1R2 set to flip all, flipping pyramidal nitrogens set to true, intramolecular hydrogen bonds set to true, protonated carboxylic acids set to flip and fix rotatable bonds set to none. Clustering of the 100 poses was performed and the top poses in large clusters at 2 Å were considered and the interactions with the protein analysed.

Synthetic reagents and instrumentation: Synthetic reagents were from Sigma-Aldrich, Combi-Blocks or Enamine and were used without further purification. Reactions were monitored by thin layer chromatography performed on plates containing Merck aluminium-backed silica gel 60 F254 (0.2 mm), and visualisation was achieved by KMnO₄ stain or UV light. Flash column chromatography

was performed with Sinaflash® P60 40–65 μm silica gel. NMR spectra were recorded at 298 K on Bruker Avance III 300, 400 and 600 MHz instruments. IR spectra were recorded on a Cary 630 FTIR spectrophotometer with a single-bounce diamond ATR accessory. HRMS data were recorded on an Orbitrap LTQ XL ion trap mass spectrometer in positive ion mode using an electrospray ionisation (ESI) source. Melting points were determined using an SRS MPA100 OptiMelt melting point apparatus.

Synthesis of *VH18*: γ -Aminobutyric acid (103 mg, 1.00 mmol) was added to a solution of **19** (187 mg, 1.14 mmol) in dry toluene (8 mL), and the resulting mixture was heated at 140 °C for 24 h. After cooling to rt, the mixture was washed with 1 M HCl (3 \times 10 mL) and brine (10 mL) and dried with MgSO_4 . The solvent was evaporated to yield a yellow-white solid (173 mg, 70%); m.p. 116.8–117.0 °C; ^1H NMR (400 MHz, CDCl_3) δ 6.28 (t, J = 1.7 Hz, 2H), 3.54 (t, J = 7.2 Hz, 2H), 3.27 (m, 2H), 2.68 (s, 2H), 2.37 (t, J = 7.2 Hz, 2H), 1.89 (tt, J = 7.2, 7.4 Hz, 2H), 1.51 (dt, J = 9.9, 1.7 Hz, 1H), 1.20 (d, J = 9.9 Hz, 1H); data in accordance with literature values.⁵⁵

Synthesis of *21*: Carbonyldiimidazole (1.48 g, 9.12 mmol) was added to a solution of 3-chloro-4-fluorobenzoic acid (1.22 g, 7.01 mmol) in THF (10 mL) and the mixture was stirred at rt for 3 h. The mixture was added dropwise to 50–60% hydrazine hydrate (2 mL, 20.6 mmol) and the mixture was stirred overnight. The solvent was evaporated and the crude product was carried on to the next step without further purification.

Synthesis of *22*: *S*-Methylisothiurea hemisulfate (194 mg, 1.39 mmol) was added to a solution of intermediate **21** (259 mg) in aqueous NaOH (1% w/v, 8 mL). The mixture was stirred for 48 h at rt, then for a further 2 h at 50 °C. The mixture was cooled to 0 °C, filtered and the precipitate washed with water and dried. The precipitate was purified by flash chromatography (5–30% MeOH/DCM) to yield a grey solid (45.5 mg, 14% over 2 steps); m.p. 155–156 °C; IR (neat) ν_{max} (cm^{-1}) 3489 (NH_2), 1649 (C=O); ^1H NMR (600 MHz, DMSO-d_6) δ 10.15 (br s, 1H), 8.11 (dd, J = 7.6, 1.8 Hz, 1H), 7.90 (ddd, J = 8.6, 5.0, 1.8 Hz, 1H), 7.30 (dd, J = 8.6, 8.9 Hz, 1H), 7.04 (br s, 2H), 6.77 (br s, 2H); $^{13}\text{C}\{^1\text{H}\}$ NMR (150 MHz, DMSO-d_6) δ 159.3, 158.0, 156.4, 152.9, 128.8, 127.3 (d, J = 7.1 Hz), 118.4 (d, J = 17.3 Hz), 115.7 (d, J = 20.5 Hz); HRMS (ESI, +ve) $\text{C}_8\text{H}_9\text{ClFN}_4\text{O}^+$ [$\text{M}+\text{H}^+$] requires m/z 231.0443, found 231.0440.

Synthesis of *23*: A solution of **22** (29.5 mg, 0.128 mmol) in water (4 mL) was heated at reflux for 24 h. After cooling to rt, the product was extracted with EtOAc (3 \times 5 mL), dried and the solvent evaporated to yield a white solid (18.5 mg, 68%); m.p. 242–243 °C; IR (neat) ν_{max} (cm^{-1}) 3427 (NH), 3185 (NH); ^1H NMR (600 MHz, DMSO-d_6) δ 12.20 (br s, 1H), 7.94 (dd, J = 6.1, 1.8 Hz, 1H), 7.84 (ddd, J = 8.8, 6.1, 1.8 Hz, 1H), 7.45 (t, J = 8.8 Hz, 1H), 6.15 (br s, 2H); $^{13}\text{C}\{^1\text{H}\}$ NMR (150 MHz,

DMSO- d_6) δ 158.4, 158.0, 156.8, 150.6, 127.5, 126.5 (d, J = 7.1 Hz), 120.1 (d, J = 18.6 Hz), 117.6 (d, J = 20.4 Hz); HRMS (ESI, +ve) $C_8H_7ClFN_4^+$ $[M+H]^+$ requires m/z 213.0338, found 213.0332.

Synthesis of 25: Boc- β -alanine (97.8 mg, 0.517 mmol), HBTU (268 mg, 0.707 mmol) and Et_3N (50 μ L, 0.36 mmol) were added to a solution of **23** (54.6 mg, 0.257 mmol) in DMF (3 mL). The mixture was stirred at rt for 2.5 h then quenched with ice-cold water (3 mL). The mixture was extracted with EtOAc (3 \times 4 mL) and the organic layer was washed with 1M NaOH (2 \times 5 mL) and brine (3 \times 5 mL), dried, and the solvent was evaporated. The crude product was purified by flash chromatography (2% MeOH/DCM) to yield a white solid (32.7 mg, 33%) [regiochemistry assigned by analogy with literature⁵¹]; m.p. 162 °C; IR (neat) ν_{max} (cm^{-1}) 3470 (NH), 3383 (NH), 3133 (NH), 1712 (C=O), 1704 (C=O); 1H NMR (400 MHz, $CDCl_3$) δ 8.10 (dd, J = 7.2, 2.2 Hz, 1H), 7.91 (ddd, J = 8.7, 4.6, 2.2 Hz, 1H), 7.19 (t, J = 8.7 Hz, 1H), 6.33 (br s, 2H), 5.04 (br s, 1H), 3.58 (dt, J = 6.0, 5.8 Hz, 2H), 3.29 (t, J = 5.8 Hz, 2H), 1.43 (s, 9H); $^{13}C\{^1H\}$ NMR (150 MHz, $CDCl_3$) δ 160.3, 158.8, 158.6, 157.2, 129.5, 127.3 (d, J = 4.0 Hz), 127.0 (d, J = 7.5 Hz), 121.6 (d, J = 18.0 Hz), 117.0, 116.9, 36.3, 35.5, 31.1, 28.5; HRMS (ESI, +ve) $C_{16}H_{19}ClFN_5O_3^+$ $[M+H]^+$ requires m/z 384.1233, found 384.1232.

Solid phase extraction coupled to mass spectrometry based assays: Inhibition of the catalytic domain of PHD2 (tPHD2₁₈₁₋₄₂₆) was measured by the reported procedure.⁵² Using the C-terminal oxygenase dependent domain peptide substrate (CDD) DLDLEMLAPYIPMDDDFQL (with a C-terminal amide) and appearance of the hydroxylated peptide product in assay buffer (50 mM Tris.Cl pH 7.5, 50 mM NaCl). Titrations of compounds for IC₅₀ determinations (3-fold and 11-point IC₅₀ curves) were performed using an ECHO 550 acoustic dispenser (Labcyte) and dry dispensed into 384-well polypropylene assay plates. The final assay concentration of DMSO was kept constant at 0.5% (v/v). tPHD2₁₈₁₋₄₂₆ was at a concentration of 300 nM (2x final assay concentration) in the assay buffer and substrate was prepared in assay buffer (20 μ M ferrous iron sulfate, 200 μ M L-ascorbic acid, 10 μ M CODD and 20 μ M 2-oxoglutarate); 25 μ L of tPHD2₁₈₁₋₄₂₆ was dispensed across each 384-well assay plate. tPHD2₁₈₁₋₄₂₆ was equilibrated with compounds for 15 minutes and the enzyme reaction initiated by 25 μ L dispense of substrate; incubations were for 15 minutes. Reaction was quenched by 10% (v/v) formic acid (5 μ L). Assay plates were transferred to a RapidFire RF365 sampling robot (Agilent) connected to an Agilent 6550 quadrupole-time-of-flight (Q-TOF) mass spectrometer, aspirated under vacuum, then loaded onto a C4 solid phase extraction (SPE) cartridge. The C4 SPE cartridge was washed with 0.1% (v/v) formic acid in water to remove non-volatile buffer salts. The peptide was then eluted from the SPE with 85% acetonitrile, 15% water containing 0.1% (v/v) formic acid into the mass spectrometer. Peptide charge states were monitored in the positive ion mode and peak area data

integrated using RapidFire Integrator software (Agilent). The % conversion of the CDD to the +16 hydroxylated product was calculated using:

$$\% \text{ conversion} = 100 \times \text{hydroxylated} / (\text{hydroxylated} + \text{non-hydroxylated peptide})$$

IC₅₀ data were determined from non-linear regression plots using GraphPad prism 6.0. The level of +16 (methionine residue oxidation) as observed in the no enzyme control was $\leq 5\%$. All data were normalized to a no enzyme control.

Cell culture: Human-derived undifferentiated neuroblastoma cells (SH-SY5Y, 94030304, Sigma Aldrich, St Louis, MO, USA) were chosen as the *in vitro* model based on their capacity to undergo oxidative stress among other cell death mechanisms^{56,57} and were cultured as per Lizarme et al.⁵⁶ with modifications. Cells were maintained at 37 °C, 5% CO₂ in a humidified incubator using media containing 43.5% Dulbecco's Modified Eagle's Medium (DMEM, 11960044), 43.5% Ham's nutrient mixture F12 (31765035), 10% Fetal Bovine Serum (FBS, P9423), 1% antibiotic/antimycotic (15240096), 1% sodium pyruvate (11360070) and 1% glutaMAX supplement (35050061). Cells were passaged with 0.05% trypsin/EDTA solution (25399962); harvested cells were recombined with suspension cells and centrifuged at 700 rpm for 4 min at room temperature. Cells were resuspended in complete media at the desired passage dilution. All cell culture reagents were obtained from Life Technologies (Mulgrave, VIC, Australia) with the exception of FBS and Minimum Essential Medium Eagle (MEM, M2279) being supplied by Sigma Aldrich (St Louis, MO, USA). All treatments and vehicle were made up in MEM from stocks.

Cell viability assay: Cells were harvested when 85–95% confluent and seeded at a density of 3×10^3 cells/mL, in complete media in Costar 96-well plates (3599, Corning Inc, Corning, NY, USA) for the MTT cell viability assay. Cells were treated and cell viability was determined using MTT assay 24 h after insult treatment, as per Lizarme et al.⁵⁶ with modifications. MTT (0.1 mg/mL; M5655, Sigma Aldrich, St Louis, MO, USA) was incubated with cells for 3 h at 37 °C, 5% CO₂ in a humidified incubator. Media was removed and the formazan product dissolved in dimethyl sulfoxide (DMSO, D8418, Sigma Aldrich, St Louis, MO, USA). Plates were shaken for 30 min and read at 570 nm using FLUOstar optima microplate reader (BMG Labtech, Ortenberg, Germany). Data was normalised against 100% viability control (MEM as vehicle) and 0% viability control (0.25% triton-X 100, 234729, Sigma Aldrich, St Louis, MO, USA).

Cell injury and protective treatments: Cells were treated with 50 μM H₂O₂ (7722841, ThermoFisher, Waltham, MA, USA), to induce oxidative stress. Cell viability was assessed by MTT assay. SH-SY5Y cells were treated with compounds **8** or **16** (Specs, Bleiswijkseweg, Zoetermeer, Netherlands).

Cell treatments were made up in the following solvents: 100% DMSO stock solution. Relevant DMSO parallel control dilutions were made to account for any toxic or protective effects of DMSO alone. Compounds **8** and **16** alone were tested for toxicity (1–100 μ M each) in MTT assay. The effect of 2 h pre-treatment with compound **8** (3 μ M, 10 μ M) or compound **16** (10–50 μ M) against 50 μ M H₂O₂ was assessed using phase-contrast microscopy and counting dead cells.

ACKNOWLEDGEMENTS

NR thanks the Australian Government for an Australian Postgraduate Award and the Mark Wainwright Analytical Centre at UNSW. CJS and AT thank the Wellcome Trust and Cancer Research UK for financial support. The authors thank William Figg Jr. for performing the expression and purification of the PHD2 used in this study.

REFERENCES

1. Wilber, R. L. Application of Altitude/Hypoxic Training by Elite Athletes. *Med. Sci. Sport. Exerc.* **39**, 1610–1624 (2007) <https://doi.org/10.1249/mss.0b013e3180de49e6>.
2. Kim, S. & Yang, E. Recent Advances in Developing Inhibitors for Hypoxia-Inducible Factor Prolyl Hydroxylases and Their Therapeutic Implications. *Molecules* **20**, 20551–20568 (2015) <https://doi.org/10.3390/molecules201119717>.
3. Fraisl, P., Aragonés, J. & Carmeliet, P. Inhibition of oxygen sensors as a therapeutic strategy for ischaemic and inflammatory disease. *Nature Reviews Drug Discovery* vol. 8 139–152 (2009) <https://doi.org/10.1038/nrd2761>.
4. Navarrete-Opazo, A., Alcayaga, J., Sepúlveda, O., Rojas, E. & Astudillo, C. Repetitive Intermittent Hypoxia and Locomotor Training Enhances Walking Function in Incomplete Spinal Cord Injury Subjects: A Randomized, Triple-Blind, Placebo-Controlled Clinical Trial. *J. Neurotrauma* **34**, 1803–1812 (2017) <https://doi.org/10.1089/neu.2016.4478>.
5. Wang, H. *et al.* Intermittent Hypoxia Training for Treating Mild Cognitive Impairment: A Pilot Study. *Am. J. Alzheimers. Dis. Other Dement.* **35**, (2020) <https://doi.org/10.1177/1533317519896725>.
6. Nguyen, H. L., Ruhoff, A. M., Fath, T. & Jones, N. M. Hypoxic postconditioning enhances

functional recovery following endoneurial-1 induced middle cerebral artery occlusion in conscious rats. *Exp. Neurol.* **306**, 177–189 (2018) <https://doi.org/10.1016/j.expneurol.2018.05.018>.

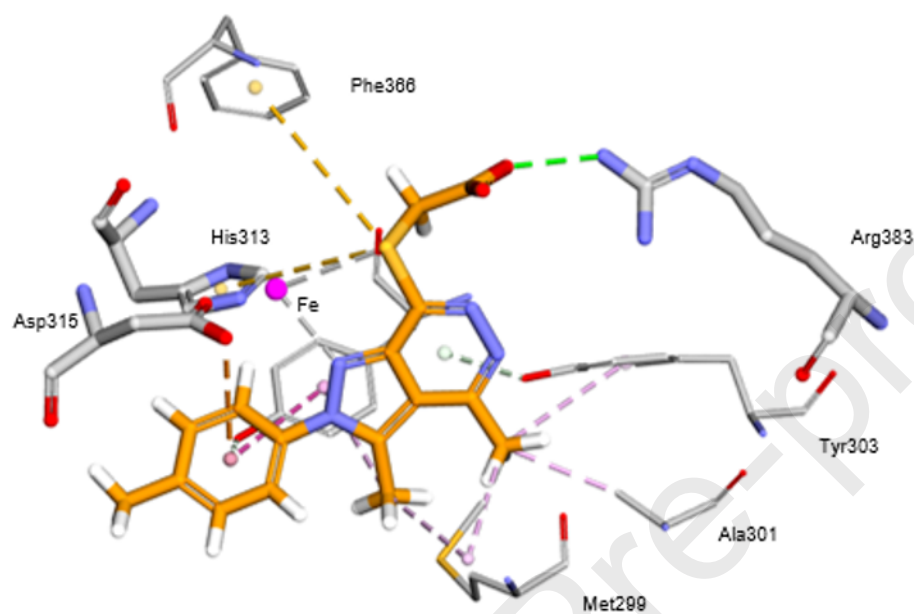
7. Lee, P., Chandel, N. S. & Simon, M. C. Cellular adaptation to hypoxia through hypoxia inducible factors and beyond. *Nature Reviews Molecular Cell Biology* vol. 21 268–283 (2020) <https://doi.org/10.1038/s41580-020-0227-y>.
8. The Nobel Prize in Physiology or Medicine 2019 - Advanced information - NobelPrize.org. <https://www.nobelprize.org/prizes/medicine/2019/advanced-information/>.
9. Wang, G. L., Jiang, B. H., Rue, E. A. & Semenza, G. L. Hypoxia-inducible factor 1 is a basic-helix-loop-helix-PAS heterodimer regulated by cellular O₂ tension. *Proc. Natl. Acad. Sci. U. S. A.* **92**, 5510–5514 (1995) <https://doi.org/10.1073/pnas.92.12.5510>.
10. Wang, G. L. & Semenza, G. L. Purification and characterization of hypoxia-inducible factor. *J. Biol. Chem.* **270**, 1230–1237 (1995) <https://doi.org/10.1074/jbc.270.3.1230>.
11. Ke, Q. & Costa, M. Hypoxia-inducible factor-1 (HIF-1). *Molecular Pharmacology* vol. 70 1469–1480 (2006) <https://doi.org/10.1124/mol.106.027029>.
12. Semenza, G. L., Neifelt, M. K., Chi, S. M. & Antonarakis, S. E. Hypoxia-inducible nuclear factors bind to an enhancer element located 3' to the human erythropoietin gene. *Proc. Natl. Acad. Sci. U. S. A.* **88**, 5680–5684 (1991) <https://doi.org/10.1073/pnas.88.13.5680>.
13. Jiang, B. H., Rue, E., Wang, G. L., Roe, R. & Semenza, G. L. Dimerization, DNA binding, and transactivation properties of hypoxia-inducible factor 1. *J. Biol. Chem.* **271**, 17771–17778 (1996) <https://doi.org/10.1074/jbc.271.30.17771>.
14. Carrero, P. *et al.* Redox-Regulated Recruitment of the Transcriptional Coactivators CREB-Binding Protein and SRC-1 to Hypoxia-Inducible Factor 1 α . *Mol. Cell. Biol.* **20**, 402–415 (2000) <https://doi.org/10.1128/mcb.20.1.402-415.2000>.
15. De Almodovar, C. R., Lambrechts, D., Mazzone, M. & Carmeliet, P. Role and therapeutic potential of VEGF in the nervous system. *Physiological Reviews* vol. 89 607–648 (2009) <https://doi.org/10.1152/physrev.00031.2008>.
16. Lange, C., Storkebaum, E., De Almodóvar, C. R., Dewerchin, M. & Carmeliet, P. Vascular endothelial growth factor: A neurovascular target in neurological diseases. *Nature Reviews*

17. Zechariah, A. *et al.* Vascular endothelial growth factor promotes pericyte coverage of brain capillaries, improves cerebral blood flow during subsequent focal cerebral ischemia, and preserves the metabolic penumbra. *Stroke* **44**, 1690–1697 (2013) <https://doi.org/10.1161/STROKEAHA.111.000240>.
18. Heeschen, C. *et al.* Erythropoietin is a potent physiologic stimulus for endothelial progenitor cell mobilization. *Blood* **102**, 1340–1346 (2003) <https://doi.org/10.1182/blood-2003-01-0223>.
19. Liu, K. *et al.* Effects of erythropoietin on blood-brain barrier tight junctions in ischemia-reperfusion rats. *J. Mol. Neurosci.* **49**, 369–379 (2013) <https://doi.org/10.1007/s12031-012-9883-5>.
20. Papandreou, I., Cairns, R. A., Fontana, L., Lim, A. L. & Denko, N. C. HIF-1 mediates adaptation to hypoxia by actively downregulating mitochondrial oxygen consumption. *Cell Metab.* **3**, 187–197 (2006) <https://doi.org/10.1016/j.cmet.2006.01.012>.
21. Vemula, S. *et al.* A functional role for sodium-dependent glucose transport across the blood-brain barrier during oxygen glucose deprivation. *J. Pharmacol. Exp. Ther.* **328**, 487–495 (2009) <https://doi.org/10.1124/jpet.108.146589>.
22. Li, L., Saliba, P., Reischl, S., Marti, H. H. & Kunze, R. Neuronal deficiency of HIF prolyl 4-hydroxylase 2 in mice improves ischemic stroke recovery in an HIF dependent manner. *Neurobiol. Dis.* **91**, 221–235 (2016) <https://doi.org/10.1016/j.nbd.2016.03.018>.
23. Takeda, K., Cowan, A. & Fong, G. H. Essential role for prolyl hydroxylase domain protein 2 in oxygen homeostasis of the adult vascular system. *Circulation* **116**, 774–781 (2007) <https://doi.org/10.1161/CIRCULATIONAHA.107.701516>.
24. Jaakkola, P. *et al.* Targeting of HIF- α to the von Hippel-Lindau ubiquitylation complex by O₂-regulated prolyl hydroxylation. *Science (80-.).* **292**, 468–472 (2001) <https://doi.org/10.1126/science.1059796>.
25. Ivan, M. *et al.* HIF α targeted for VHL-mediated destruction by proline hydroxylation: Implications for O₂ sensing. *Science (80-.).* **292**, 464–468 (2001) <https://doi.org/10.1126/science.1059817>.

26. Masson, N., William, C., Maxwell, P. H., Fugh, C. W. & Ratchine, P. J. <Masson-2001-Independent function.pdf>. **20**, 5197–5206 (2001) <https://doi.org/10.1093/emboj/20.18.5197>.
27. Rabinowitz, M. H. Inhibition of Hypoxia-Inducible Factor Prolyl Hydroxylase Domain Oxygen Sensors: Tricking the Body into Mounting Orchestrated Survival and Repair Responses. (2013) doi:10.1021/jm400386j <https://doi.org/10.1021/jm400386j>.
28. McNeill, L. A. *et al.* The use of dioxygen by HIF prolyl hydroxylase (PHD1). *Bioorganic Med. Chem. Lett.* **12**, 1547–1550 (2002) [https://doi.org/10.1016/S0960-894X\(02\)00219-6](https://doi.org/10.1016/S0960-894X(02)00219-6).
29. Flashman, E. *et al.* Evidence for the slow reaction of hypoxia-inducible factor prolyl hydroxylase 2 with oxygen. *FEBS J.* **277**, 4089–4099 (2010) <https://doi.org/10.1111/j.1742-4658.2010.07804.x>.
30. Chowdhury, R. *et al.* Structural basis for oxygen degradation domain selectivity of the HIF prolyl hydroxylases. *Nat. Commun.* **7**, 1–10 (2016) <https://doi.org/10.1038/ncomms12673>.
31. Karuppagounder, S. S. & Ratan, R. R. Hypoxia-inducible factor prolyl hydroxylase inhibition: Robust new target or another big bust for stroke therapeutics. *Journal of Cerebral Blood Flow and Metabolism* vol. 32 1347–1361 (2012) <https://doi.org/10.1038/jcbfm.2012.28>.
32. Kim, S. Y. & Yang, E. G. Recent advances in developing inhibitors for hypoxia-inducible factor prolyl hydroxylases and their therapeutic implications. *Molecules* vol. 20 20551–20568 (2015) <https://doi.org/10.3390/molecules201119717>.
33. Naser, M. *et al.* A review on iron chelators in treatment of iron overload syndromes. *Int. J. Hematol. stem cell Res.* **10**, 239–247 (2016).
34. Guo, C. *et al.* Deferoxamine-mediated up-regulation of HIF-1 α prevents dopaminergic neuronal death via the activation of MAPK family proteins in MPTP-treated mice. *Exp. Neurol.* **280**, 13–23 (2016) <https://doi.org/10.1016/j.expneurol.2016.03.016>.
35. Guo, C. *et al.* Intranasal deferoxamine attenuates synapse loss via up-regulating the P38/HIF-1 α pathway on the brain of APP/PS1 transgenic mice. *Front. Aging Neurosci.* **7**, (2015) <https://doi.org/10.3389/fnagi.2015.00104>.
36. Yeh, T. L. *et al.* Molecular and cellular mechanisms of HIF prolyl hydroxylase inhibitors in clinical trials. *Chem. Sci.* **8**, 7651–7668 (2017) <https://doi.org/10.1039/c7sc02103h>.

37. Eitzschig, H. K., Bratton, D. L. & Colgan, S. P. Targeting hypoxia signalling for the treatment of ischaemic and inflammatory diseases. *Nature Reviews Drug Discovery* vol. 13 852–869 (2014) <https://doi.org/10.1038/nrd4422>.
38. Locatelli, F., Fishbane, S., Block, G. A. & MacDougall, I. C. Targeting Hypoxia-Inducible Factors for the Treatment of Anemia in Chronic Kidney Disease Patients. *American Journal of Nephrology* vol. 45 187–199 (2017) <https://doi.org/10.1159/000455166>.
39. Chan, M. C. *et al.* Potent and selective triazole-based inhibitors of the hypoxia-inducible factor prolyl-hydroxylases with activity in the murine brain. *PLoS One* **10**, (2015) <https://doi.org/10.1371/journal.pone.0132004>.
40. Pajouhesh, H. & Lenz, G. R. Medicinal chemical properties of successful central nervous system drugs. *NeuroRx* **2**, 541–553 (2005) <https://doi.org/10.1602/neurorx.2.4.541>.
41. Mikitsh, J. L. & Chacko, A. M. Pathways for small molecule delivery to the central nervous system across the blood-brain barrier. *Perspect. Medicin. Chem.* **6**, 11–24 (2014) <https://doi.org/10.4137/PMc.s13384>.
42. Liao, C., Sitzmann, M., Pugliese, A. & Nicklaus, M. C. Software and resources for computational medicinal chemistry. *Future Medicinal Chemistry* vol. 3 1057–1085 (2011) <https://doi.org/10.4155/fmc.11.63>.
43. Wolber, G. & Langer, T. LigandScout: 3-D pharmacophores derived from protein-bound ligands and their use as virtual screening filters. *J. Chem. Inf. Model.* **45**, 160–169 (2005) <https://doi.org/10.1021/ci049885e>.
44. Ambure, P., Kar, S. & Roy, K. Pharmacophore mapping-based virtual screening followed by molecular docking studies in search of potential acetylcholinesterase inhibitors as anti-Alzheimer's agents. *BioSystems* **116**, 10–20 (2014) <https://doi.org/10.1016/j.biosystems.2013.12.002>.
45. Chen, Z. *et al.* Pharmacophore-based virtual screening versus docking-based virtual screening: A benchmark comparison against eight targets. *Acta Pharmacol. Sin.* **30**, 1694–1708 (2009) <https://doi.org/10.1038/aps.2009.159>.
46. Lagorce, D., Sperandio, O., Baell, J. B., Miteva, M. A. & Villoutreix, B. O. FAF-Drugs3: a web server for compound property calculation and chemical library design. *Web Serv. issue Publ. online* **43**, (2015) <https://doi.org/10.1093/nar/gkv353>.

47. Whitty, A. Growing PAINS in academic drug discovery. *Future Medicinal Chemistry* vol. 5 797–801 (2011) <https://doi.org/10.4155/fmc.11.44>.
48. Best, M., Degen, A., Baalman, M., Schmidt, T. T. & Wombacher, R. Two-Step Protein Labeling by Using Lipoic Acid Ligase with Norbornene Substrates and Subsequent Inverse-Electron Demand Diels-Alder Reaction. *ChemBioChem* **16**, 1158–1162 (2015) <https://doi.org/10.1002/cbic.201500042>.
49. Boraie, A. T. A., El Ashry, E. S. H. & Duerkop, A. Regioselectivity of the alkylation of S-substituted 1,2,4-triazoles with dihaloalkanes. *Chem. Cent. J.* **10**, 1–13 (2016) <https://doi.org/10.1186/s13065-016-0165-0>.
50. Fidler, Z. N. *et al.* Acyl derivatives of 3-amino-1,2,4-triazole. *Chem. Heterocycl. Compd.* **16**, 1079–1083 (1980) <https://doi.org/10.1007/BF00496616>.
51. Dzygiel, A., Masiukiewicz, E. & Rzeszutarska, B. Acetylation of 5-amino-1H-[1,2,4]triazole revisited. *J. Agric. Food Chem.* **50**, 1383–1388 (2002) <https://doi.org/10.1021/jf010734a>.
52. Holt-Martyn, J. P. *et al.* Structure-Activity Relationship and Crystallographic Studies on 4-Hydroxypyrimidine HIF Prolyl Hydroxylase Domain Inhibitors. *ChemMedChem* vol. 15 270–273 (2020) <https://doi.org/10.1002/cmdc.201900557>.
53. Chowdhury, R. *et al.* Selective small molecule probes for the hypoxia inducible factor (HIF) Prolyl Hydroxylases. *ACS Chem. Biol.* **8**, 1488–1496 (2013) <https://doi.org/10.1021/cb400088q>.
54. McDonough, M. A. *et al.* Cellular oxygen sensing: Crystal structure of hypoxia-inducible factor prolyl hydroxylase (PHD2). *Proc. Natl. Acad. Sci. U. S. A.* **103**, 9814–9819 (2006) <https://doi.org/10.1073/pnas.0601283103>.
55. Liu, J. *et al.* ‘Brush-first’ method for the parallel synthesis of photocleavable, nitroxide-labeled poly(ethylene glycol) star polymers. *J. Am. Chem. Soc.* **134**, 16337–16344 (2012) <https://doi.org/10.1021/ja3067176>.
56. Lizarne, Y. *et al.* Synthesis and neuroprotective activity of dictyoquinazol A and analogues. *Bioorganic Med. Chem.* **24**, 1480–1487 (2016) <https://doi.org/10.1016/j.bmc.2016.02.016>.
57. Zille, M. *et al.* Ferroptosis in neurons and cancer cells is similar but differentially regulated by histone deacetylase inhibitors. *eNeuro* **6**, 263–281 (2019)



Declaration of interests

☒ The authors declare that they have no known competing financial interests or personal relationships that could have appeared to influence the work reported in this paper.

☐ The authors declare the following financial interests/personal relationships which may be considered as potential competing interests: